In vivo long-term voltage imaging by genetically encoded voltage indicator reveals spatiotemporal dynamics of neuronal populations during development.

Asuka Shiraishi[1], Ayane Hayashi[2], Narumi Fukuda[1], Mari Hishinuma[1], Hiroaki Miyazawa[1], Sachiko Tsuda[1§]

1 Division of Life Science, Graduate School of Science and Engineering, Saitama University, 255 Shimo-Okubo, Sakura-ku, Saitama City, Saitama 338-8570, Japan

2 Department of Regulatory Biology, Faculty of Science, Saitama University, 255 Shimo-Okubo, Sakura-ku, Saitama City, Saitama 338-8570, Japan

[§]Author for correspondence (stsuda@mail.saitama-u.ac.jp)

Abstract

A central question in brain development lies in how individual neurons emerge and organize communities to acquire various functions. Voltage imaging provides unique approaches to addressing this by enabling simultaneous, non-invasive, in vivo recording of voltage dynamics from a population of cells. Recently, genetically encoded voltage indicators (GEVIs) facilitate cell-type specific imaging of voltage dynamics. However, it has not been applied to brain development. Here, we applied ArcLight, a GEVI utilizing voltage-sensitive domain, to zebrafish and established experimental approaches for analyzing voltage and morphology of neuron populations during development, focusing on the spinal cord and cerebellum. We initially demonstrated that Arclight was widely distributed in the neural tissues. With voltage imaging, we successfully visualized the coordinated, spontaneous activity of spinal cord neurons in their early stage of development at a high spatiotemporal resolution, at subcellular and population levels. Hyperpolarization and subthreshold signals were also detected. Finally, long-term voltage imaging during development revealed the process of changes in voltage dynamics in neuron populations, accompanied by axonal outgrowth. Voltage imaging could greatly contribute to our understanding of the functional organization of the nervous system during development.

Introduction

The nervous system consists of a large number of neurons that perform various functions. During development, these neurons are generated and communicate with each other to form functional networks. For deeper understanding of brain function and development, it is essential to understand how the brain is formed and organized. However, such attempts are often hindered by the vast number of neurons. Optical methods provide a powerful approach to solving these difficulties because light facilitates non-invasive access to many neurons, which is difficult with electrophysiological techniques.

Voltage imaging enables fast, direct, and simultaneous detection of membrane potentials in a population of neurons, providing an excellent system for circuit analysis [1-3]. Its high speed and directness allow the detection of action potentials, hyperpolarization, and subthreshold responses, which are difficult to examine using calcium imaging, partly because of the slow kinetics of the indicators and the dynamics of calcium [4, 5]. Voltage imaging began with activity recording using voltage-sensitive dyes (VSDs) [6]. Subsequently, various types of VSDs have been developed to improve the brightness, signal-to-noise ratio (SNR), and wider variations in color, expanding our understanding of network dynamics and development in various brain regions [7-11]. In recent years, the development of genetically encoded voltage indicators (GEVIs) has progressed rapidly, resulting in cell-type-specific voltage imaging, which is difficult to achieve with VSDs. This yielded GEVIs with faster kinetics and brighter fluorescence, overcoming prior weaknesses in the speed and SNR [12-14]. There are several types of GEVIs, based on their structures. One is a mosaic protein that uses the voltage-sensitive domain of voltage-sensitive phosphatases [15-18]. Another class of GEVIs uses the voltage sensitivity of microbial rhodopsins [19-22]. These GEVIs have been applied to the study of brain function for various brain regions [23-27]. However, in most studies, GEVI voltage imaging was used to undermine the function of neural circuits, and very few attempts have been made to understand brain development.

In this study, to examine the dynamics of neuronal populations and their development, we applied ArcLight to zebrafish, and established a series of

recording approaches to expand the power of voltage imaging in developmental biology. Zebrafish is an optimal model system for embryology and neuroscience. The transparent and relatively small brain of zebrafish, together with various transgenic lines, provides an excellent system for analyzing the functional organization of the brain in various behavioral modalities by the whole-brain recordings [28, 29]. Several GEVIs have been successfully used for voltage imaging of the zebrafish brain, mainly to analyze the circuit functions [21, 22, 25, 26, 30]. In this study, we focus on the spinal cord and cerebellum, which are suitable for studying neural circuit development because of their rapid development, ease of observation, and accumulated information on circuit organization [31, 32].

The spinal cord contains neural circuits that play fundamental roles in locomotion. These circuits drive coordinated movements of the left and right sides of the body by a central pattern generator, which is a fundamental element of locomotion [33]. At an early stage of development, this coordinated activity emerges as the spontaneous firing of spinal cord neurons, which is considered important for circuit formation [34]. Although electrophysiological and optical studies have elucidated the firing dynamics of these neurons, the mechanisms by which this coordinated activity emerges remain to be understood [35-37]. This transient activity, known as fetal movement in mammals, has been observed as coiling movements during early development in zebrafish. In the spinal cord, this process leads to periodic bursts of alternating populations of neurons on the left and right sides [38, 39]. Previous studies have shown that such activity patterns emerge from uncorrelated activities within a few hours of early development [36, 39-41]. However, the mechanisms by which individual neurons emerge and constitute network function remain unclear. This is partly because previous studies have used either electrophysiology or calcium imaging, creating a gap between the information on the synaptic profiles of individual neurons obtained by electrophysiology and the population information obtained by calcium imaging. To solve this issue, we need to obtain voltage information from a population of neurons during the course of development.

Cumulative information has been obtained on cerebellar circuits, which play pivotal roles in motor coordination, learning, and cognition, and are evolutionally highly conserved [31, 42]. Inhibition and high-frequency activity are prominent in the cerebellum and contribute to various adaptive properties of the cerebellum, including long-term depression and modular development of the cerebellar circuitry [43-47]. In contrast to VSD imaging, which has long been used to uncover cerebellar circuit dynamics, the use of GEVI in the cerebellum, particularly in its developmental process, is still limited [11, 21, 25, 44, 48].

Materials and Methods

Fish lines

Wild-type zebrafish (Danio rerio) with RW genetic background or nacre line were used [49]. Tg(elavl3:GAL4-VP16), Tg(hspGFFDMC28C;UAS:RFP), Tg(gSA2AzGFF152B;UAS:RFP), and Tg(UAS:lynRFP) fish lines have been described previously and obtained from the National BioResource Project [25, 50, 51]. The Tg lines were crossed with the nacre line. All procedures were performed in accordance with a protocol approved by the Saitama University Committee on Animal Research.

DNA Construction and establishment of ArcLight transgenic line

To generate pTol2-UAS-ArcLight plasmid, ArcLight-A242 sequence was excited from the pCS2-ArcLight-A242 plasmid (Addgene) and inserted into pTol2-UAS-MCSF-polyA, in which UAS and polyA sequences were integrated into the pTol2-MCS plasmid [52]. pTol2-Aldoca-ArcLight-Q239-polyA construct was generated using a Purkinje cell-specific promoter, aldorace C, and the ArcLight-Q239 sequence. The ArcLight-Q239 and aldorace sequences were extracted from pCS2-ArcLight-Q239 and aldoca-5k-pGEM-T, respectively, and inserted into pTol2-UAS-MCSF-polyA pDNA. To establish pTol2-UAS-ArcLight line, Tol2 plasmid DNA and *transposase* mRNA were co-injected into one-cell-stage embryos. Genotyping was performed using the primers for ArcLight-A242 (5′-TCGACGGTATCGATAAGCTTGC-3′,5′- CACCTCCCCCTGAACCTGAAACATA-

136 3′).
137
138 **Transient expression of ArcLight in the spinal cord and cerebellum**
139 For the spinal cord, 25 ng/μl pTol2-UAS-ArcLight-A242-polyA plasmid DNA was
140 co-injected with 25 ng/μl *Tol2 transposase* mRNA into one-cell-stage embryos of
141 Tg(elavl3:GAL4-VP16) embryos, which express Gal4 in neurons [53]. After the
142 injection, the embryos were incubated at 23°C and then transferred to 28°C by
143 18 hour post fertilization (hpf). ArcLight-positive embryos were screened at the
144 18.5 to 19 hpf, followed by voltage imaging of the spinal cord at 20 to 24 hpf. For
145 the cerebellum, 5-40 ng/μl pTol2-aldoca-ArcLight-Q239-polyA plasmid DNA was
146 co-injected with 25 ng/μl *Tol2 transposase* mRNA into one-cell-stage nacre
147 embryos. ArcLight-positive embryos were screened at 4 to 5 days post
148 fertilization (dpf), followed by voltage imaging at 5 to 6 dpf.
149
150 **Confocal imaging**
151 Zebrafish embryos were paralyzed in 0.02% tricaine and mounted on 2% low
152 melting-point agarose (Sigma-Aldrich). Optical sectioning was performed using
153 an Olympus FV1000 or a Nikon A1R (detector: A1-DU4) confocal microscope.
154 ImageJ, NIS-Elements (Nikon), and Imaris (Bitplane) programs were used to
155 perform the image analysis.
156
157 **Voltage imaging of the spinal cord**
158 Embryos from 16 to 23 hpf were paralyzed with tubocurarine (0.5 mM, Sigma-
159 Aldrich), with their tail tips cut for better penetration of tubocurarine [39, 54]. Then,
160 embryos were mounted on 1.8% low melting-point agarose containing 0.1-0.2
161 mM tubocurarine. After embedding the embryos onto 1% agarose, an
162 extracellular solution (134 mM NaCl, 2.9 mM KCl, 2.1 mM $CaCl_2$, 1.2 mM $MgCl_2$,
163 10 mM HEPES, and 10 mM glucose, adjusted to pH 7.8 with NaOH) containing
164 150 mM tubocurarine was added. The agarose around the tail was removed using
165 a surgical blade to allow efficient transfer of the drug solution. For high-speed
166 voltage imaging, a fluorescence microscope (FN-1, Nikon) equipped with a
167 CMOS camera (ORCA-Flash4.0, Hamamatsu Photonics) was used with a

40×/0.8 NA water-immersion lens. For most recordings, a 0.7× relay lens (NIKON) was also used. Fluorescence images were acquired using NIS-Elements (Nikon) software at approximately 16-200 Hz. High-speed confocal scanning was performed using a confocal microscope (Nikon A1R) with a 25×/1.0 NA water-immersion lens. For drug treatment, tetrodotoxin (1 μM, TOCRIS) was added to the extracellular solution using a peristaltic pump (World Precision Instruments). A thermo plate was used to keep the recording chamber at 28°C (Tokai hit).

Voltage imaging of the cerebellum

Embryos from 5 to 9 dpf were paralyzed with 0.02% tricaine and transferred to an extracellular solution. Next, the embryos were mounted on 2% low melting-point agarose. For imaging, a fluorescence microscope (FN-1, Nikon) equipped with a CMOS camera (ORCA-Flash4.0, Hamamatsu Photonics) was used with a 40×/0.8 NA water-immersion lens. Fluorescent images were acquired using NIS-Elements or HCImage (Hamamatsu Photonics) at approximately 50–200 Hz.

Image analysis

Images were analyzed using the NIS-Elements (Nikon), Fiji, and OriginPro (Lightstone) programs as described previously [54]. To extract changes in fluorescence intensity, regions of interest (ROIs) were manually set using NIS-element software (Nikon). Normalized changes in fluorescence intensity in the target regions (ROIs) were quantitatively analyzed by calculating dF/F in the ROIs ($dF/F_0=[F_{(t)}–F_0]/F_0$, where $F_{(t)}$ and F_0 are the fluorescence intensities at a certain time point and initial time points, respectively). If the larvae/embryos moved during the voltage imaging, the images were aligned using a Fiji program (TurboReg plugin). Denoising and bleach corrections were also applied to some data using OriginPro (Lightstone). Cross-correlation and hierarchical clustering analyses were performed using OriginPro (Lightstone).

Results

200 **Establishment of the ArcLight zebrafish line**

201 To examine neuronal activity in the developing brain using voltage imaging, GEVI
202 ArcLight was used to establish transgenic zebrafish lines via the GAL4-UAS and
203 Tol2 transposon systems [29]. We generated a pTol2-UAS-ArcLight-A242-polyA
204 construct and established a transgenic line (Fig. 1a, b). To test whether ArcLight
205 was localized to the cellular membranes in Tg(UAS:ArcLight) fish, we observed
206 Tg(elavl3:GAL4-VP16;UAS:ArcLight;UAS:lyn-RFP) embryos, in which gal4 was
207 expressed in neurons, and the cellular membranes were labeled with Lyn-RFP.
208 At 1 dpf, ArcLight was widely observed in the neural tube and co-localized with
209 Lyn-RFP, indicating that ArcLight was properly distributed on the cellular
210 membrane in the neural tube (Fig. 1b, c). The distribution of ArcLight was also
211 examined in other brain regions, such as the cerebellum, using transgenic lines
212 expressing gal4 specifically in cerebellar neurons. Confocal imaging showed that
213 ArcLight was clearly expressed in granule cells and inferior olive neurons, which
214 are key components of cerebellar circuits [42] (Supplementary Figs. S1 and S2).
215 These results indicate that ArcLight is expressed in various neuron types in
216 developing zebrafish.

217

218 **ArcLight could detect neural activity at the population and single-cell levels**

219 Next, we performed high-speed imaging of the spinal cord of the Tg(elavl3:GAL4-
220 VP16;UAS:ArcLight) embryos. Spinal cord neurons show spontaneous firing at
221 the early stage of development, and this coordinated activity of the neuronal
222 populations begins at 17 hpf [36, 40, 41]. As shown in Figure 1, oscillatory
223 changes in ArcLight fluorescence intensity were detected in the ventral region of
224 somites 3–8 at 20 hpf at a frequency of 0.14±0.10 Hz (6 fish, Fig. 1d–g). Phases
225 of fluorescent changes differed between the left and right sides of the spinal cord
226 and occurred alternately, which is consistent with previous reports showing
227 periodic depolarization (PD) of spinal cord neurons (Warp et al., 2012). This
228 activity mostly disappeared after treatment with the sodium channel blocker
229 tetrodotoxin (TTX) (Fig. 1e-g; left side: control 0.14±0.10 Hz, TTX 0.01±0.02 Hz,
230 $p<0.05$, right side: control 0.14±0.10 Hz, TTX 0.01±0.02 Hz, $p<0.05$, Wilcoxon

signed-rank test, 6 fish). These data indicated that ArcLight can detect spontaneous activity in developing zebrafish spinal cord neurons.

Next, we examined whether ArcLight enables the detection of neural activity at the single-cell and population levels. Figure 2 shows an example of voltage imaging of the spinal cord. The oscillatory activity was clearly detected in each neuron, and differences in the size and pattern of activity between neighboring neurons were visualized using ArcLight (Fig. 2a and b, 35 fish). Many of these depolarizations occurred sequentially along the rostrocaudal axis. In addition to large depolarizations that closely resembled PD, slight membrane potential fluctuations were also observed between the PDs (Fig. 2c). Their timing and patterns suggest that they represent a subthreshold activity called a synaptic burst, which has been reported in electrophysiological recordings [38]. Cross-correlation analysis revealed a strong positive correlation between the ipsilateral neurons and a negative correlation between the contralateral neurons (Fig. 2d). This result indicates that membrane potential changes are highly synchronized between neurons on the ipsilateral side of the spinal cord at the single-cell level, and that they alternate between the left and right sides. Furthermore, the hierarchical clustering analysis suggested that populations of neurons on the same side exhibited higher synchrony (Fig. 2e).

High-spatiotemporal voltage imaging at the subcellular level in the spinal cord

Measuring membrane potential dynamics at the level of neuronal compartments such as axons and dendrites is important for understanding information processing in the brain [55, 56]. To record the cell bodies and axons of the spinal cord neurons, Tg(elavl3:GAL4-VP16;UAS:ArcLight) embryos between 20 and 23 hpf were observed from their side (Fig. 3a). We focused on primary motor neurons (PMNs), as they are easy to observe because of their distinguished morphology (Fig. 3a and Supplementary Fig. S3). As shown in Figure 3, we successfully performed wide-field voltage imaging and detected the membrane potential in the soma and proximo/distal regions of the axons (13 fish). The soma and axons showed similar patterns of depolarization, but the size of the

membrane potential fluctuations might be slightly smaller in the axons than in the cell soma (Fig. 3b). The depolarization of the axons was also detected by using confocal microscopy (Supplementary Fig. S3). Furthermore, recordings at a higher spatial resolution enabled the illumination of filopodia dynamics and voltage changes (Supplementary Fig. S4). Interestingly, we noticed that there were areas within the axon where the amplitude of the membrane potential dynamics was larger than that of the others (Supplementary Fig. S4).

Single-cell labeling of neurons by ArcLight enables simultaneous observation of morphology and activity

Spinal cord circuits consist of many types of neurons whose position, morphology, and physiological properties vary [57]. To uncover the circuit dynamics and its development, it is essential to observe the morphology and voltage dynamics of each neuron. For this purpose, the Tg(elavl3:GAL4-VP16;UAS:ArcLight) line has a weakness in that neighboring neurons also express ArcLight, making it challenging to observe the morphology of individual cells. Therefore, we obtained both recordings by expressing ArcLight in a mosaic manner.

By injecting UAS-ArcLight pDNA into Tg(elavl3:GAL4-VP16) fish, we obtained embryos in which spinal cord neurons were sparsely labeled by ArcLight, enabling precise detection of the dynamics of membrane potentials (Fig. 4a–c, 20 hpf, PMNs). We also succeeded in recording interneurons that were otherwise difficult to identify (Fig. 4d and e). In addition to PD and SB-like activity, some neurons exhibited hyperpolarization (Fig. 4e). In contrast to cells 2 and 3, cell 1 did not show depolarization. In one hour, these neurons changed their morphology (Supplementary Fig. S5). These results indicate that voltage imaging using ArcLight enables measurement of the voltage dynamics of neurons at various levels (population, single cell, and subcellular), providing a powerful approach for analyzing neural circuits.

Sparse labeling of cerebellar neurons by ArcLight was also achieved by injecting UAS-ArcLight pDNA into gal4 lines. We could detect ArcLight expression in the axons (climbing fibers) and soma of the inferior olive neurons, which have a critical role in cerebellar learning (Supplementary Fig. S2b). We also attempted

295 to perform voltage imaging of cerebellar Purkinje cells, which play pivotal roles in
296 the cerebellum. By injecting ArcLight pDNA, which drives the expression of
297 ArcLight specifically in Purkinje cells, we obtained embryos with sparse labeling
298 of Purkinje cells (Supplementary Fig. S7a and b). Voltage imaging at 5 dpf
299 revealed a change in fluorescence intensity, indicative of depolarization in
300 Purkinje cells (Supplementary Fig. S7b–d). However, significant bleaching makes
301 long-term imaging difficult, and the membrane potential could not be recorded
302 from multiple Purkinje cells.
303
304 **Developmental changes in the membrane potentials of spinal neurons**
305 Next, we examined the developmental changes in voltage dynamics in neuron
306 populations. The periodic firing observed in the spinal cord of zebrafish embryos
307 corresponds to coiling behavior, which is suggested to be essential for circuit
308 formation [34]. During embryogenesis, this characteristic activity appears at
309 approximately 17 hpf and rapidly increases in frequency and amplitude until 20
310 hpf, followed by a gradual decrease [36]. However, the mechanism by which the
311 cooperative activity of this population of spinal neurons emerges and changes
312 during development remains unclear. To investigate voltage dynamics in
313 populations of spinal cord neurons, we performed voltage imaging of zebrafish
314 embryos during this developmental period.
315 As shown in Figure 5, voltage imaging was successfully performed for the first
316 time from the developing spinal cord continuously from 18 to 20 hpf (Fig. 5). At
317 18 hpf, a PMN located in the eight somite region had an axonal structure but
318 seldom exhibited burst activity. Instead, it often showed fluctuations in the voltage
319 signal (Fig. 5c, cell 1). This neuron gradually extended its axons, increasing the
320 number of burst firings at 18.5 hpf. By 19.5 hpf, the firing frequency quickly
321 reached 0.35 Hz. In the same embryo, we also obtained a recording from the
322 PMN located in 10 somite region (Fig. 5c, cell 2). At 18 hpf, cell 2 exhibited a short
323 protrusion near its soma, suggesting that it had just started extending an axon.
324 Cell 2 appeared to have almost no activity at 18 hpf but started to show
325 depolarization at 18.5 hpf. However, the pattern of membrane potential fluctuation
326 was quite different from that of mature PMNs, with many cells showing a slower

rise in depolarization. Additionally, small fluctuations in membrane potentials were continuously detected, raising the possibility that they might reflect subthreshold dynamics of membrane potentials in PMNs (Fig. 5c). By 19.5 hpf, cell2 extended the axon, while the frequency of bursts rapidly increased to 0.35 Hz. A similar pattern of changes in voltage dynamics was also observed in the soma of cell 2 and in other embryos (Supplementary Fig. S6, 5 fish, 20 cells). These findings suggest that the coordinated activity in the spinal cord develops through multiple steps: (1) no firing, (2) small depolarization (initiation of axon outgrowth), (3) irregular cooperative activity, and (4) cooperative activity.

Next, we examined how the spontaneous activity in the spinal cord changes over time. Voltage imaging was performed from 20 to 23 hpf (Fig. 6; Supplementary Fig. S8). The results showed that the regular and rapid population activity observed at 20 hpf decreased by 23 hpf. The pattern of depolarization also changed, with the bursts becoming longer in duration and losing alternating activity (Fig. 6b). Cross-correlation analysis revealed that at 20 hpf, ipsilateral and contralateral pairs of neurons showed a high degree of synchrony and periodicity (Fig. 6c). However, at 23 hpf, they seemed to reduce, except that ipsilateral pairs maintained their synchrony. As for the coordination between left and right, at 20–21 hpf, almost all neurons showed alternating activity. At 23–24 hpf, this was significantly reduced to nearly 80% (Fig. 6d; 20–21 hpf: 98.9±1.10%; 23–24 hpf: 98.9±1.10%, 5 fish; 23–24 hpf: 79.8%±5.71%, 4 fish; $p<0.05$, Mann–Whitney U test). These results indicate that periodic activity and left-right coordination decrease later in development, but the synchrony in ipsilateral neurons remains.

Discussion

GEVI voltage imaging is useful as it enables the recording of membrane potentials from many specific neuronal cell types noninvasively without using electrodes. However, it has not been applied to studying neurogenesis. In this study, we established experimental methods to enhance voltage imaging in the zebrafish cerebellum and spinal cord. These are important not only for analyzing

neural circuits but also for revealing developmental mechanisms.

Previously, electrophysiological recordings have been used to characterize membrane dynamics in the spinal cord. However, neurons were observed for a short period due to the invasive nature of the recordings. In addition, recordings were limited to single cells [57, 58]. Moreover, developmental analysis was performed using calcium imaging; however, in principle, it is impossible to record membrane potential dynamics using this method [39-41]. To the best of our knowledge, this is the first report of visualizing membrane potential dynamics in genetically defined neuronal populations during spinal cord development. Similarly, we believe that this is the first example of long-term GEVI-based imaging of neural circuit formation during development.

Voltage imaging of spinal cord neural circuits

In this study, we successfully established a transgenic zebrafish line expressing ArcLight. Initially, we focused on the spinal cord: one of the earliest circuits to emerge during development, consisting of a relatively limited number of neurons [36]. Voltage imaging at 20 hpf showed that the spinal neuronal population exhibited regular, alternating left-right synchronous activity. The obtained patterns were clear, with similar patterns of voltage changes to those recorded by electrophysiology, but with higher resolution than those previously recorded using ASAP1 or calcium imaging (Miyazawa et al., 2018; Muto et al., 2011; Wan et al., 2019; Warp et al., 2012). This would probably be because ArcLight has faster kinetics than the calcium sensor, and shows a higher SNR than ASAP1 [14, 59]. Previously, electrophysiological studies showed that most of the spinal cord neurons at the stage exhibit periodic bursts of activity called PD that drives tail-coiling behaviors (equivalent to human fetal movements). Similar patterns of burst firing, similar firing frequency, and the importance of sodium channel all support the notion that the observed depolarization represents PD.

In addition to these suprathreshold activities, subthreshold activities, such as SB and hyperpolarization, were also detected by ArcLight, further highlighting the use of voltage imaging. While further analysis is needed, including simultaneous electrophysiological recordings with voltage imaging, this is the first non-invasive

imaging of voltage dynamics in a spinal cord neurons population at their early stage of development.

High-resolution voltage imaging

Subcellular information is important, because neuronal functions are regulated at the subcellular level, for instance, in dendritic computation and axonal compartments [55, 56]. Here we showed that ArcLight allowed recording from the cell body and axon compartments of PMNs. In some cells, we noticed slightly larger voltage changes at the distal region of axons. This may be due in part to the non-uniform distribution of sodium channels [56]. In addition, filopodia and lamellipodia were labeled by ArcLight, with filopodia also showing voltage dynamics. Further research is desirable to understand the role of voltage changes in filopodia; for instance, in synapse formation and plasticity. Also, further extension of this technique to ratiometry voltage imaging is necessary for more accurate recording [60]. The ability to simultaneously and noninvasively observe cell morphology and activity allows a deeper understanding of network dynamics and their formation.

Emergence and changes in spinal cord networks during development

Long-term voltage imaging in the spinal cord showed that regular cooperative activity parallels axon outgrowth. For instance, PMNs were found to mature through multiple steps: (1) no firing, (2) small depolarization (initiation of axon outgrowth), (3) irregular cooperative activity, and (4) cooperative activity. This process proceeds in the same order in neurons distributed along the roster-caudal axis. Although it is known that spinal cord neurons without axonal outgrowth do not fire, this is the first time that stage-dependent changes in voltage have been demonstrated in the same population of spinal cord neurons [57].

Notably, PMNs exhibited small fluctuations in membrane potentials before starting regular depolarization. In early-stage of spinal cord development, ion channels and gap junctions are known to be key in driving voltage dynamics in spinal cord neurons, whereas the contribution of chemical synapses is limited to glycinergic ones [36]. Since electrical coupling is a powerful source of

synchronous activity, it would be interesting if the small fluctuations in membrane potentials reflect electrical coupling [43, 61, 62]. Simple neuronal circuits connected by gap junctions are one of the key regulators in animal behavior [63]. Further research is desirable to determine whether the observed small depolarization contains, for instance, spikelets. Furthermore, more evidence is necessary on other important questions; whether pattern generators exist, where they are located, and how they facilitate network activity [41]. Our approach with in vivo voltage imaging could provide further information.

Voltage imaging in the cerebellum

In the cerebellum, cumulative information on circuit dynamics was collected by voltage-sensitive dye imaging [10, 48, 64, 65]. To further understand circuit dynamics, optical recording of membrane potentials in a cell-type-specific manner is desirable. However, no study has clearly described cell-type-specific voltage imaging using GEVIs, despite several systems being available for neuron-type-specific expression [51]. In this study, we obtained strong ArcLight expression in cerebellar granule cells and inferior olive neurons. As for Purkinje cells, a central neuron in the cerebellum, we obtained ArcLight positive Purkinje cells only by the transient expression system. By voltage imaging, spontaneous depolarization was detected in Purkinje cells. We assumed that this depolarization represents complex spikes (CS), one of the key firing patterns of Purkinje cells, since the frequency was similar to that of CSs detected by cell-attached electrophysiological recordings at the same developmental stage in zebrafish [66]. However, we could not detect simple spikes (SSs) in Purkinje cells; this would partly be because SSs exhibit smaller amplitude and higher frequencies, making them more difficult to target with this imaging [67, 68]. To improve the SNR of the recordings, stronger drivers for increasing GEVI expression, more sensitive sensors, and an improved illumination/recording system are desirable [14, 21, 69]. Although further validation with electrophysiology is required, this work will provide an important step forward in understanding information processing and development in the cerebellum.

Regarding GEVI expression, we noticed considerable differences in intensity

between neuron types, similar to other GEVIs such as ASAP1 [25]. To expand GEVI voltage imaging for the analysis of various neuron types, it is essential to examine this difference in expression efficiency and to solve this issue.

In conclusion, this is the first report of simultaneous and non-invasive recordings of membrane potentials from neuronal populations during development using a GEVI. Based on the imaging system that we established in zebrafish, we would be able to further understand how complex activity and behaviors emerge from small populations of neurons by combining cell-type-specific recordings with manipulations of neuronal activity through optical, electrophysiological, and genetic approaches. Furthermore, our approach would help elucidate the bioelectric signals in various biological phenomena, including morphogenesis [70, 71].

Acknowledgement

We thank Drs M. Hibi, K. Kawakami, S. Higashijima, H. Okamoto, H. Kakinuma, and R. Amo for providing fish lines and constructs, and J. Nakai, M. Ohkura, K. Ando, K. Yamasu, L. Cohen, Y. Bando, S. Fukushima for technical supports and helpful discussion. This work was supported in part by JSPS KAKENHI (Grants-in-Aid for Scientific Research), JST Tenure Track program at Saitama University (SUTT), Strategic Research Program for Brain Science from Ministry of Education, Culture, Sports, Science, and Technology of Japan (ASTEP), Kao Foundation grant, Asahi Glass Foundation, and Kato-bio Foundation.

Author Contributions

A.S. and S.T. conceived and designed the experiments. A.S, A.H., N.F., M.H., K.M., and S.T. performed the experiments. S.T., A.S., and N.F. wrote the manuscript. All authors reviewed the manuscript.

Additional Information

Competing interests

The authors declare no competing interests.

Data Availability

All data generated or analyzed in this study are included in the manuscript and supporting files.

References

1. Cohen, L.B. and B.M. Salzberg, *Optical measurement of membrane potential.* Rev Physiol Biochem Pharmacol, 1978. **83**: p. 35-88.
2. Loew, L.M., et al., *Evidence for a charge-shift electrochromic mechanism in a probe of membrane potential.* Nature, 1979. **281**(5731): p. 497-9.
3. Djurisic, M., et al., *Optical monitoring of neural activity using voltage-sensitive dyes.* Methods Enzymol, 2003. **361**: p. 423-51.
4. Lin, M.Z. and M.J. Schnitzer, *Genetically encoded indicators of neuronal activity.* Nat Neurosci, 2016. **19**(9): p. 1142-53.
5. Homma, R., et al., *Wide-field and two-photon imaging of brain activity with voltage- and calcium-sensitive dyes.* Philos Trans R Soc Lond B Biol Sci, 2009. **364**(1529): p. 2453-67.
6. Ross, W.N., et al., *Changes in absorption, fluorescence, dichroism, and Birefringence in stained giant axons: : optical measurement of membrane potential.* J Membr Biol, 1977. **33**(1-2): p. 141-83.
7. Yan, P., et al., *Palette of fluorinated voltage-sensitive hemicyanine dyes.* Proc Natl Acad Sci U S A, 2012. **109**(50): p. 20443-8.
8. Wuskell, J.P., et al., *Synthesis, spectra, delivery and potentiometric responses of new styryl dyes with extended spectral ranges.* J Neurosci Methods, 2006. **151**(2): p. 200-15.
9. Momose-Sato, Y., T. Nakamori, and K. Sato, *Spontaneous depolarization wave in the mouse embryo: origin and large-scale propagation over the CNS identified with voltage-sensitive dye imaging.* Eur J Neurosci, 2012. **35**(8): p. 1230-41.
10. Rokni, D., R. Llinas, and Y. Yarom, *Stars and stripes in the cerebellar cortex: a voltage sensitive dye study.* Front Syst Neurosci, 2007. **1**: p. 1.
11. Roome, C.J. and B. Kuhn, *Dendritic coincidence detection in Purkinje neurons of awake mice.* Elife, 2020. **9**.
12. Storace, D., et al., *Toward Better Genetically Encoded Sensors of Membrane Potential.* Trends Neurosci, 2016. **39**(5): p. 277-289.
13. Kannan, M., G. Vasan, and V.A. Pieribone, *Optimizing Strategies for Developing Genetically Encoded Voltage Indicators.* Front Cell Neurosci, 2019. **13**: p. 53.
14. Bando, Y., et al., *Comparative Evaluation of Genetically Encoded Voltage Indicators.* Cell Rep, 2019. **26**(3): p. 802-813 e4.
15. Akemann, W., et al., *Imaging neural circuit dynamics with a voltage-sensitive fluorescent protein.* J Neurophysiol, 2012. **108**(8): p. 2323-37.
16. Jin, L., et al., *Single action potentials and subthreshold electrical events imaged*

529 *in neurons with a fluorescent protein voltage probe.* Neuron, 2012. **75**(5): p. 779-
530 85.
531 17. St-Pierre, F., et al., *High-fidelity optical reporting of neuronal electrical activity with*
532 *an ultrafast fluorescent voltage sensor.* Nat Neurosci, 2014. **17**(6): p. 884-9.
533 18. Tsutsui, H., et al., *Improving membrane voltage measurements using FRET with*
534 *new fluorescent proteins.* Nat Methods, 2008. **5**(8): p. 683-5.
535 19. Hochbaum, D.R., et al., *All-optical electrophysiology in mammalian neurons*
536 *using engineered microbial rhodopsins.* Nat Methods, 2014. **11**(8): p. 825-33.
537 20. Gong, Y., et al., *High-speed recording of neural spikes in awake mice and flies*
538 *with a fluorescent voltage sensor.* Science, 2015. **350**(6266): p. 1361-6.
539 21. Abdelfattah, A.S., et al., *Bright and photostable chemigenetic indicators for*
540 *extended in vivo voltage imaging.* Science, 2019. **365**(6454): p. 699-704.
541 22. Piatkevich, K.D., et al., *A robotic multidimensional directed evolution approach*
542 *applied to fluorescent voltage reporters.* Nat Chem Biol, 2018. **14**(4): p. 352-360.
543 23. Nakajima, R. and B.J. Baker, *Mapping of excitatory and inhibitory postsynaptic*
544 *potentials of neuronal populations in hippocampal slices using the GEVI, ArcLight.*
545 J Phys D Appl Phys, 2018. **51**(50).
546 24. Storace, D.A. and L.B. Cohen, *Measuring the olfactory bulb input-output*
547 *transformation reveals a contribution to the perception of odorant concentration*
548 *invariance.* Nat Commun, 2017. **8**(1): p. 81.
549 25. Miyazawa, H., et al., *Optical interrogation of neuronal circuitry in zebrafish using*
550 *genetically encoded voltage indicators.* Sci Rep, 2018. **8**(1): p. 6048.
551 26. Bohm, U.L., et al., *Voltage imaging identifies spinal circuits that modulate*
552 *locomotor adaptation in zebrafish.* Neuron, 2022. **110**(7): p. 1211-1222 e4.
553 27. Yang, H.H., et al., *Subcellular Imaging of Voltage and Calcium Signals Reveals*
554 *Neural Processing In Vivo.* Cell, 2016. **166**(1): p. 245-57.
555 28. Ahrens, M.B., et al., *Brain-wide neuronal dynamics during motor adaptation in*
556 *zebrafish.* Nature, 2012. **485**(7399): p. 471-7.
557 29. Asakawa, K., et al., *Genetic dissection of neural circuits by Tol2 transposon-*
558 *mediated Gal4 gene and enhancer trapping in zebrafish.* Proc Natl Acad Sci U S
559 A, 2008. **105**(4): p. 1255-60.
560 30. Yoshimatsu, T., et al., *Ancestral circuits for vertebrate color vision emerge at the*
561 *first retinal synapse.* Sci Adv, 2021. **7**(42): p. eabj6815.
562 31. Hashimoto, M. and M. Hibi, *Development and evolution of cerebellar neural*
563 *circuits.* Dev Growth Differ, 2012. **54**(3): p. 373-89.
564 32. McLean, D.L., et al., *A topographic map of recruitment in spinal cord.* Nature,
565 2007. **446**(7131): p. 71-5.

566 33. Grillner, S., *Neurobiological bases of rhythmic motor acts in vertebrates.* Science,
567 1985. **228**(4696): p. 143-9.
568 34. Menelaou, E., et al., *Embryonic motor activity and implications for regulating*
569 *motoneuron axonal pathfinding in zebrafish.* Eur J Neurosci, 2008. **28**(6): p. 1080-
570 96.
571 35. Fidelin, K. and C. Wyart, *Inhibition and motor control in the developing zebrafish*
572 *spinal cord.* Curr Opin Neurobiol, 2014. **26C**: p. 103-109.
573 36. Saint-Amant, L., *Development of motor rhythms in zebrafish embryos.* Prog Brain
574 Res, 2010. **187**: p. 47-61.
575 37. O'Donovan, M.J., *The origin of spontaneous activity in developing networks of*
576 *the vertebrate nervous system.* Curr Opin Neurobiol, 1999. **9**(1): p. 94-104.
577 38. Saint-Amant, L. and P. Drapeau, *Motoneuron activity patterns related to the*
578 *earliest behavior of the zebrafish embryo.* J Neurosci, 2000. **20**(11): p. 3964-72.
579 39. Muto, A., et al., *Genetic visualization with an improved GCaMP calcium indicator*
580 *reveals spatiotemporal activation of the spinal motor neurons in zebrafish.* Proc
581 Natl Acad Sci U S A, 2011. **108**(13): p. 5425-30.
582 40. Warp, E., et al., *Emergence of patterned activity in the developing zebrafish*
583 *spinal cord.* Curr Biol, 2012. **22**(2): p. 93-102.
584 41. Wan, Y., et al., *Single-Cell Reconstruction of Emerging Population Activity in an*
585 *Entire Developing Circuit.* Cell, 2019. **179**(2): p. 355-372 e23.
586 42. Ito, M., *Cerebellar circuitry as a neuronal machine.* Prog Neurobiol, 2006. **78**(3-
587 5): p. 272-303.
588 43. Mann-Metzer, P. and Y. Yarom, *Electrotonic coupling interacts with intrinsic*
589 *properties to generate synchronized activity in cerebellar networks of inhibitory*
590 *interneurons.* J Neurosci, 1999. **19**(9): p. 3298-306.
591 44. Cohen, D. and Y. Yarom, *Patches of synchronized activity in the cerebellar cortex*
592 *evoked by mossy-fiber stimulation: questioning the role of parallel fibers.* Proc
593 Natl Acad Sci U S A, 1998. **95**(25): p. 15032-6.
594 45. Whittington, M.A., R.D. Traub, and J.G. Jefferys, *Synchronized oscillations in*
595 *interneuron networks driven by metabotropic glutamate receptor activation.*
596 Nature, 1995. **373**(6515): p. 612-5.
597 46. Ito, M., *Cerebellar long-term depression.* Trends Neurosci, 1996. **19**(1): p. 11-12.
598 47. Apps, R. and R. Hawkes, *Cerebellar cortical organization: a one-map hypothesis.*
599 Nat Rev Neurosci, 2009. **10**(9): p. 670-81.
600 48. Tsuda, S., et al., *Probing the function of neuronal populations: combining*
601 *micromirror-based optogenetic photostimulation with voltage-sensitive dye*
602 *imaging.* Neurosci Res, 2013. **75**(1): p. 76-81.

603 49. Lister, J.A., et al., *nacre encodes a zebrafish microphthalmia-related protein that*
604 *regulates neural-crest-derived pigment cell fate.* Development, 1999. **126**(17): p.
605 3757-67.
606 50. Kimura, Y., C. Satou, and S. Higashijima, *V2a and V2b neurons are generated*
607 *by the final divisions of pair-producing progenitors in the zebrafish spinal cord.*
608 Development, 2008. **135**(18): p. 3001-5.
609 51. Takeuchi, M., et al., *Establishment of Gal4 transgenic zebrafish lines for analysis*
610 *of development of cerebellar neural circuitry.* Dev Biol, 2015. **397**(1): p. 1-17.
611 52. Nakayama, Y., et al., *Comprehensive analysis of target genes in zebrafish*
612 *embryos reveals gbx2 involvement in neurogenesis.* Dev Biol, 2017. **430**(1): p.
613 237-248.
614 53. Kimura, Y., et al., *Hindbrain V2a neurons in the excitation of spinal locomotor*
615 *circuits during zebrafish swimming.* Curr Biol, 2013. **23**(10): p. 843-9.
616 54. Hiyoshi, K., et al., *In vivo wide-field voltage imaging in zebrafish with voltage-*
617 *sensitive dye and genetically encoded voltage indicator.* Dev Growth Differ, 2021.
618 **63**(8): p. 417-428.
619 55. London, M. and M. Hausser, *Dendritic computation.* Annu Rev Neurosci, 2005.
620 **28**: p. 503-32.
621 56. Garrido, J.J., et al., *Dynamic compartmentalization of the voltage-gated sodium*
622 *channels in axons.* Biol Cell, 2003. **95**(7): p. 437-45.
623 57. Saint-Amant, L. and P. Drapeau, *Synchronization of an embryonic network of*
624 *identified spinal interneurons solely by electrical coupling.* Neuron, 2001. **31**(6):
625 p. 1035-46.
626 58. Saint-Amant, L. and P. Drapeau, *Time course of the development of motor*
627 *behaviors in the zebrafish embryo.* J Neurobiol, 1998. **37**(4): p. 622-32.
628 59. Storace, D.A., et al., *Monitoring brain activity with protein voltage and calcium*
629 *sensors.* Sci Rep, 2015. **5**: p. 10212.
630 60. Kim, B.B., et al., *A red fluorescent protein with improved monomericity enables*
631 *ratiometric voltage imaging with ASAP3.* Sci Rep, 2022. **12**(1): p. 3678.
632 61. Epsztein, J., et al., *Impact of spikelets on hippocampal CA1 pyramidal cell activity*
633 *during spatial exploration.* Science, 2010. **327**(5964): p. 474-7.
634 62. de Solages, C., et al., *High-frequency organization and synchrony of activity in*
635 *the purkinje cell layer of the cerebellum.* Neuron, 2008. **58**(5): p. 775-88.
636 63. Gutierrez, G.J., T. O'Leary, and E. Marder, *Multiple mechanisms switch an*
637 *electrically coupled, synaptically inhibited neuron between competing rhythmic*
638 *oscillators.* Neuron, 2013. **77**(5): p. 845-58.
639 64. Roome, C.J. and B. Kuhn, *Simultaneous dendritic voltage and calcium imaging*

and somatic recording from Purkinje neurons in awake mice. Nat Commun, 2018. **9**(1): p. 3388.

65. Okumura, K., et al., *Optical measurement of neuronal activity in the developing cerebellum of zebrafish using voltage-sensitive dye imaging.* Neuroreport, 2018. **29**(16): p. 1349-1354.

66. Hsieh, J.Y., et al., *Rapid development of Purkinje cell excitability, functional cerebellar circuit, and afferent sensory input to cerebellum in zebrafish.* Front Neural Circuits, 2014. **8**: p. 147.

67. Knogler, L.D., A.M. Kist, and R. Portugues, *Motor context dominates output from purkinje cell functional regions during reflexive visuomotor behaviours.* Elife, 2019. **8**.

68. Harmon, T.C., et al., *Distinct responses of Purkinje neurons and roles of simple spikes during associative motor learning in larval zebrafish.* Elife, 2017. **6**.

69. Namikawa, K., et al., *Modeling Neurodegenerative Spinocerebellar Ataxia Type 13 in Zebrafish Using a Purkinje Neuron Specific Tunable Coexpression System.* J Neurosci, 2019. **39**(20): p. 3948-3969.

70. Levin, M., *Bioelectric signaling: Reprogrammable circuits underlying embryogenesis, regeneration, and cancer.* Cell, 2021. **184**(8): p. 1971-1989.

71. Harris, M.P., *Bioelectric signaling as a unique regulator of development and regeneration.* Development, 2021. **148**(10).

662 **Figure Legends**

663

664 **Figure 1**

665 Transgenic zebrafish showing membrane-localized ArcLight and spontaneous
666 activity in the neural tube. (a) Schematic diagram of plasmid construct for ArcLight.
667 (b) Lateral views of ArcLight-expressing embryos at 1 dpf. ArcLight is distributed
668 widely in the neural tube of Tg(elavl3:GAL4-VP16;UAS:ArcLight) fish. (c) Dorsal
669 view of the neural tube of Tg(elavl3:GAL4-VP16;UAS:ArcLight;UAS:lyn-RFP)
670 embryos at 1 dpf. ArcLight (green) is co-localized with Lyn-RFP (red: cell
671 membranes) in the neural tube (arrowheads). Higher magnification images are
672 shown in the lower panel. (d-f) Spontaneous activity of spinal cord neurons is
673 detected by ArcLight imaging. (d) Dorsal view of the ventral spinal cord of Tg
674 (elavl3:GAL4-VP16;UAS:ArcLight-A242) fish at 20 hpf. The rostral side is to the
675 left, and the area between 3–8 somites is shown. A schematic diagram of the
676 imaging system is shown on the right. Changes in the fluorescence of ArcLight
677 ($-\Delta F/F_0$) are indicated by the pseudocolor scale shown at right. White
678 arrowheads indicate the activated neurons. Regions of interest (ROIs) located
679 between 5–7 somites are indicated by red (right side) and blue (left side)
680 rectangular in (d). Fluorescence changes of ArcLight in the ROIs are shown on
681 the right. The time point of the image is indicated by a black arrowhead. (f-g) The
682 spontaneous activity in the spinal cord mostly disappeared by tetrodotoxin (TTX)
683 treatment (6 fish, *: $p < 0.05$). The imaged plane and ROIs are in the same positions
684 as in (d).

685

686 **Figure 2**

687 Monitoring of spontaneous activity of individual cells in the spinal cord by ArcLight
688 imaging. (a) A fluorescence image of the ventral spinal cord of Tg(elavl3:GAL4-
689 VP16;UAS:ArcLight) fish at 21 hpf. ROIs are located at the 18 cells (red: right
690 side, blue: left side). Higher magnification views are shown on the right. (b)
691 Changes in ArcLight signals fluorescence of ArcLight at the two time points
692 indicated in (c). (c) Activity patterns of the 18 cells are shown. A higher
693 magnification view of the ArcLight signal of cell 4 is shown at the bottom. (b). (d,

694 e) Hierarchal clustering analysis of the voltage dynamics in the 18 cells shows
695 the synchronous activity in the ipsilateral neuron pairs (d), and also several
696 groups with higher synchrony within them (e).
697
698 **Figure 3**
699 Voltage imaging of spinal cord neurons at a high spatiotemporal resolution at the
700 cellular compartment level by ArcLight. (a) Lateral views of the spinal cord of
701 Tg(elavl3:GAL4-VP16;UAS:ArcLight) fish at 20 hpf. A schematic diagram of the
702 imaging system is shown on the right. (b) Changes in ArcLight signal are
703 observed at soma and axons in three different ROIs shown in (a). Higher
704 resolution observations are shown in Supplementary Fig. S3 and S4.
705
706 **Figure 4**
707 Single cell labeling of neurons by ArcLight enables simultaneous recording of
708 voltage and morphology. (a) Schematic diagram of the co-injection experiment.
709 (b) A stacked confocal image of the spinal cord region of the injected embryo at
710 20 hpf. The left side view is shown. Arrowheads and arrows indicate the soma
711 and axons of ArcLight positive cells, respectively. (c) Voltage dynamics of a
712 primary motor neuron are indicated by a yellow arrowhead in (b). ROIs at soma
713 and axons are shown in red and blue, respectively. (d, e) Voltage imaging of the
714 spinal cord interneurons. A higher magnification view is shown in (e). ArcLight
715 signals from three cells are shown on the right. In addition to periodic
716 depolarization, hyperpolarization (white arrowheads) and subthreshold-like
717 signals (black arrowheads) are observed.
718
719 **Figure 5**
720 Long-term voltage imaging of the spinal cord shows the emergence of population
721 activity. (a) Left views of the spinal cord of ArcLight positive fish from 18 hpf to
722 19.5 hpf. (b) Enlarged views of (a). (c) Voltage dynamics obtained from the axons
723 of the two cells shown in (a). Arrowheads indicate small depolarization.
724
725 **Figure 6**

726 Changes in firing properties in spinal cord neuron populations. (a) Dorsal view of
727 ArcLight positive spinal cord at 20 hpf. (b) Voltage dynamics of each neuron are
728 shown at 20 and 23 hpf. The position of ROIs is indicated in (a). (c) Cross-
729 correlation analysis of ipsilateral and contralateral pairs of spinal cord neurons at
730 20 and 23 hpf. (d) Probability of altering activity at 20-21 hpf and 23-24 hpf.
731
732
733 **Supplementary Figure S1**
734 ArcLight (green) is distributed in cerebellar granule cells (red). Dorsal view of the
735 cerebellum of Tg(hspGFFDMC152C;UAS:RFP;UAS:ArcLight) fish observed at 6
736 dpf. Higher magnification views are shown in the lower panel.
737
738 **Supplementary Figure S2**
739 ArcLight is expressed in inferior olivary neurons. (a) Dorsal view of the inferior
740 olive (IO) of Tg(hspGFFDMC28C;UAS:RFP;UAS:ArcLight) fish at 8 dpf.
741 Arrowheads in the cerebellum (CE) indicate ArcLight signals (green) in the
742 climbing fibers. (b) (left) Schematic diagram of the co-injection experiment. (right)
743 Transient expression of ArcLight in a single IO neuron. Higher magnification
744 views are shown in the right panel. ArcLight expression is observed in climbing
745 fibers (1), as well as in the soma and dendrites of an IO neuron (2).
746
747 **Supplementary Figure S3**
748 Confocal observation of ArcLight expression and voltage dynamics in the spinal
749 cord. (a) Lateral views of Tg(elavl3:GAL4-VP16;UAS:ArcLight) embryo at 1 dpf.
750 Higher magnification images shown on the right indicate filopodia and
751 lameripoidia of primary motor neurons (arrowheads). (b) Voltage imaging of cell1
752 in (a). ROIs were set at the axonal region. ArcLight detected depolarization at
753 axons (black arrowheads). The gray area is the period when the embryos moved.
754
755 **Supplementary Figure S4**
756 Voltage imaging of a primary motor neuron at higher spatial resolution. (a) Left
757 views of the spinal cord at two different time points. Arrowheads indicate filopodia

(white, yellow). A yellow arrowhead indicates a filopodium that shows a prominent extension. (b, c) An example of voltage dynamics detected at various positions in the axon. ROI4-6 were set on a filopodium. ROI 7 was set in a region where no clear structure was observed.

Supplementary Figure S5

Single-cell labeling by ArcLight shows the morphological changes of the spinal cord neurons. Images taken at 21 hpf and 22 hpf are shown. An arrowhead indicates a growth cone of the extending axon.

Supplementary Figure S6

ArcLight imaging in Purkinje cells. (a) (top) Schematic diagram ofpTo2-aldoca-ArcLightQ239-polyA construct. (bottom) ArcLight is expressed in Purkinje cells in the cerebellum (CE). Arrowheads and an arrow indicate Purkinje cell soma and dendrite, respectively. A higher magnification view is shown on the right. (b-d) ArcLight imaging exhibits depolarization in Purkinje cells. (b) ArcLight signal in the recorded Purkinje cells. (c) Depolarization signals are observed by ArcLight imaging (arrowheads). (d) Enlarged views of the traces are shown in (c).

Supplementary Figure S7

ArcLight imaging in Purkinje cells. (a) (top) Schematic diagram ofpTo2-aldoca-ArcLightQ239-polyA construct. (bottom) ArcLight is expressed in Purkinje cells in the cerebellum (CE). Arrowheads and an arrow indicate Purkinje cell soma and dendrite, respectively. A higher magnification view is shown on the right. (b-d) ArcLight imaging exhibits depolarization in Purkinje cells. (b) ArcLight signal in the recorded Purkinje cells. (c) Depolarization signals are observed by ArcLight imaging (arrowheads). (d) Enlarged views of the traces are shown in (c).

Supplementary Figure S8

Long-term voltage imaging shows the changes in the firing patterns of the spinal cord neurons population. (a) ROIs position of cells 1-6. (b) Voltage dynamics of the 6 cells are shown from 20 to 23 hpf. Cells on the right and left sides of the

spinal cord are shown in red and blue, respectively.

Supplementary Movie1

Spontaneous activity of individual cells in the spinal cord is observed by ArcLight. Dorsal view of the ventral spinal cord of Tg(elavl3:GAL4-VP16;UAS:ArcLight) fish at 21 hpf.

Supplementary Movie2

Monitoring of spontaneous activity of spinal cord neurons, including primary motor neurons by ArcLight. Left view of the spinal cord of Tg(elavl3:GAL4-VP16;UAS:ArcLight) fish at 20 hpf.

Supplementary Movie3

Single-cell labeling and voltage imaging of spinal cord neurons using ArcLight. Left view of the spinal cord of Tg(elavl3:GAL4-VP16) embryo at 21 hpf. A high-resolution image is shown in Supplementary Figure S4.

Supplementary Movie4

Voltage dynamics of an axonal region of a primary motor neuron at a high spatial resolution. Left view of the spinal cord Tg(elavl3:GAL4-VP16;UAS:ArcLight) fish at 18.5 hpf.

Figure 1

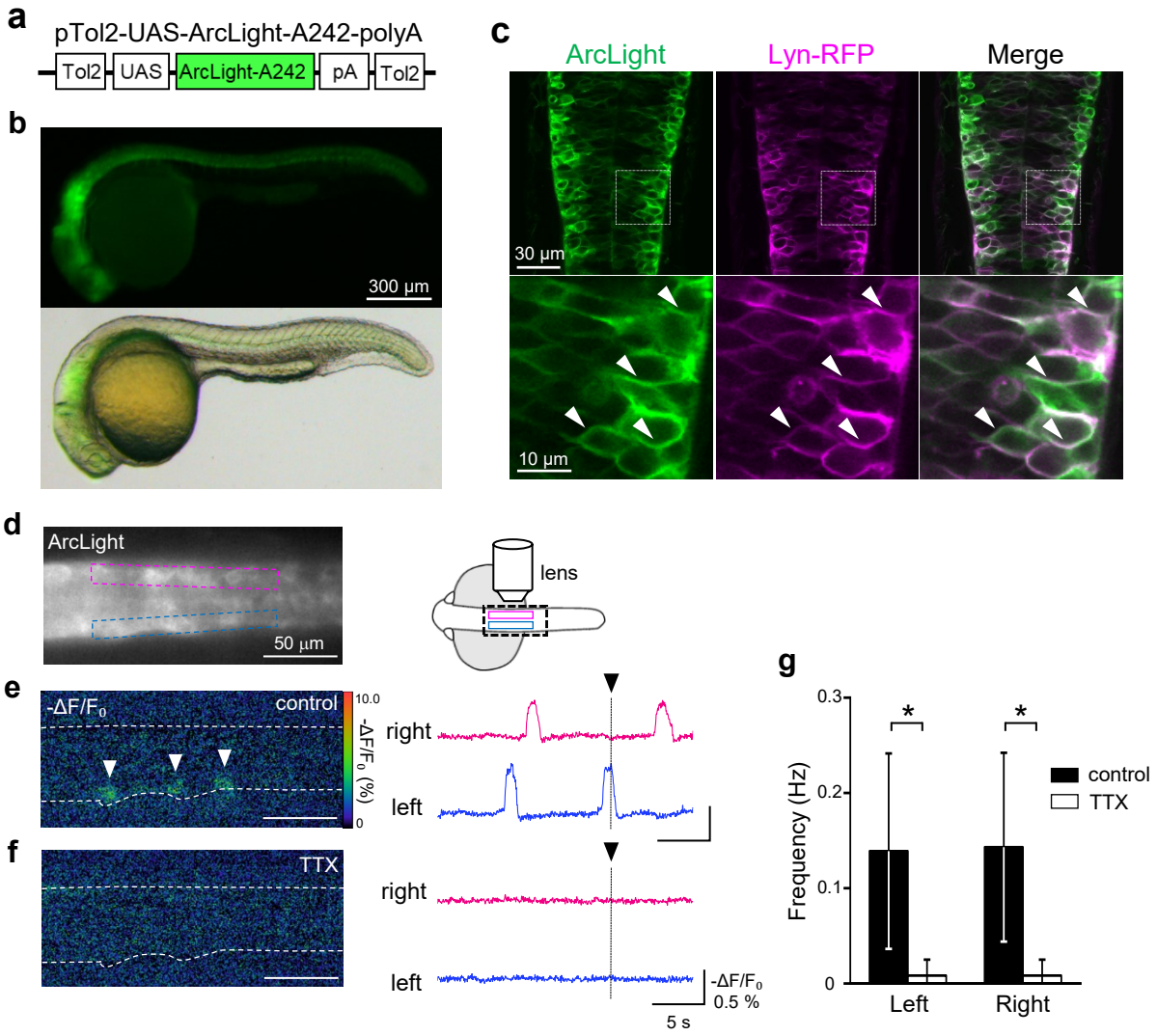
a
pTol2-UAS-ArcLight-A242-polyA
Tol2
UAS
ArcLight-A242
pA
Tol2
b
300 μm
c
ArcLight
Lyn-RFP
Merge
30 μm
10 μm
d
ArcLight
50 μm
lens
e
-ΔF/F0
control
10.0
-ΔF/F0 (%)
0
right
left
f
TTX
right
left
-ΔF/F0
0.5 %
5 s
g
0.3
0.2
0.1
0
Frequency (Hz)
*
*
control
TTX
Left
Right

Figure 2

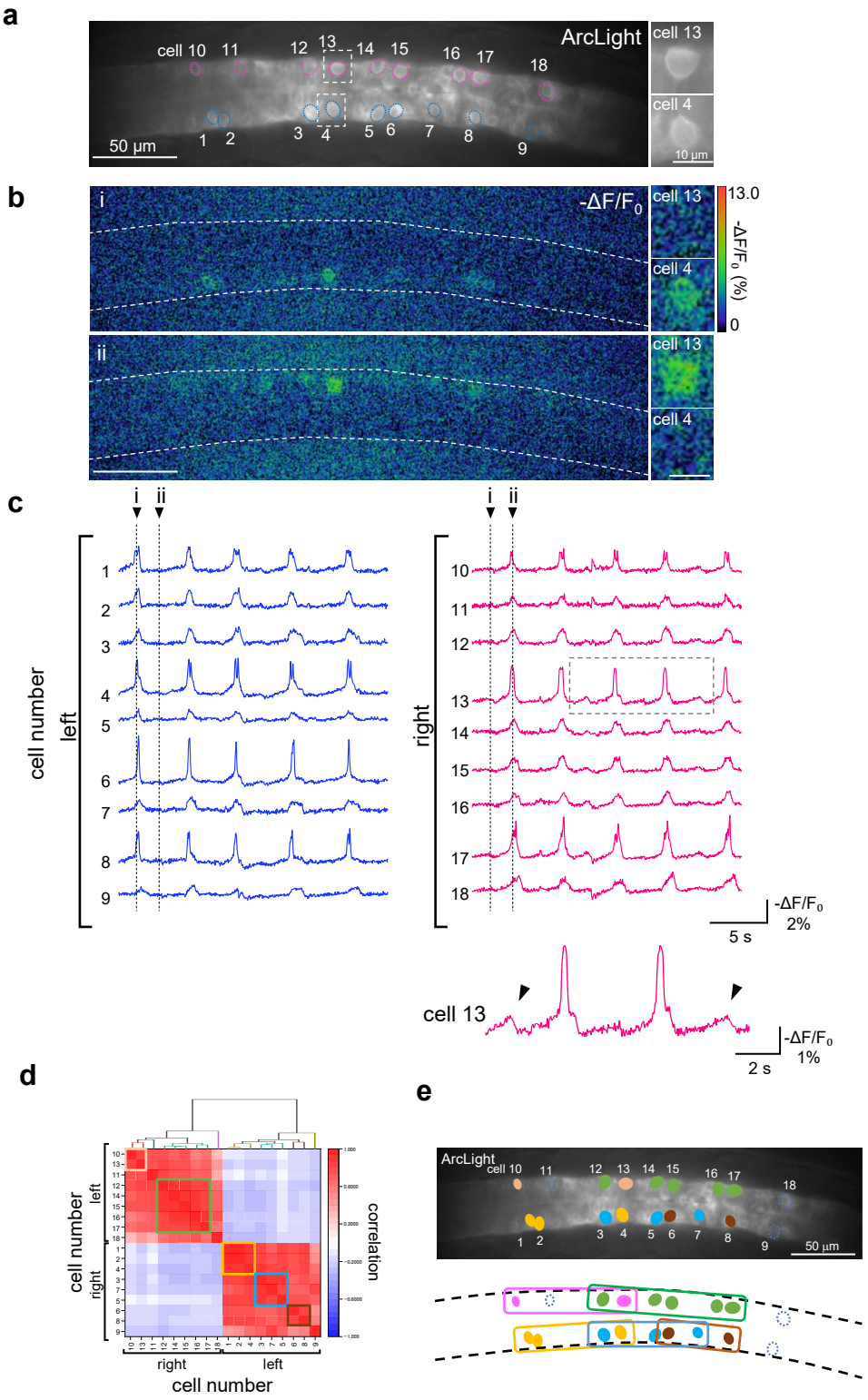
a
ArcLight
cell 10
11
12
13
14
15
16
17
18
1
2
3
4
5
6
7
8
9
50 µm
cell 13
cell 4
10 µm
b
i
ii
-ΔF/F0
cell 13
cell 4
13.0
-ΔF/F0 (%)
0
c
cell number
left
right
-ΔF/F0
2%
5 s
cell 13
-ΔF/F0
1%
2 s
d
cell number
left
right
correlation
e
ArcLight
50 µm

Figure 3

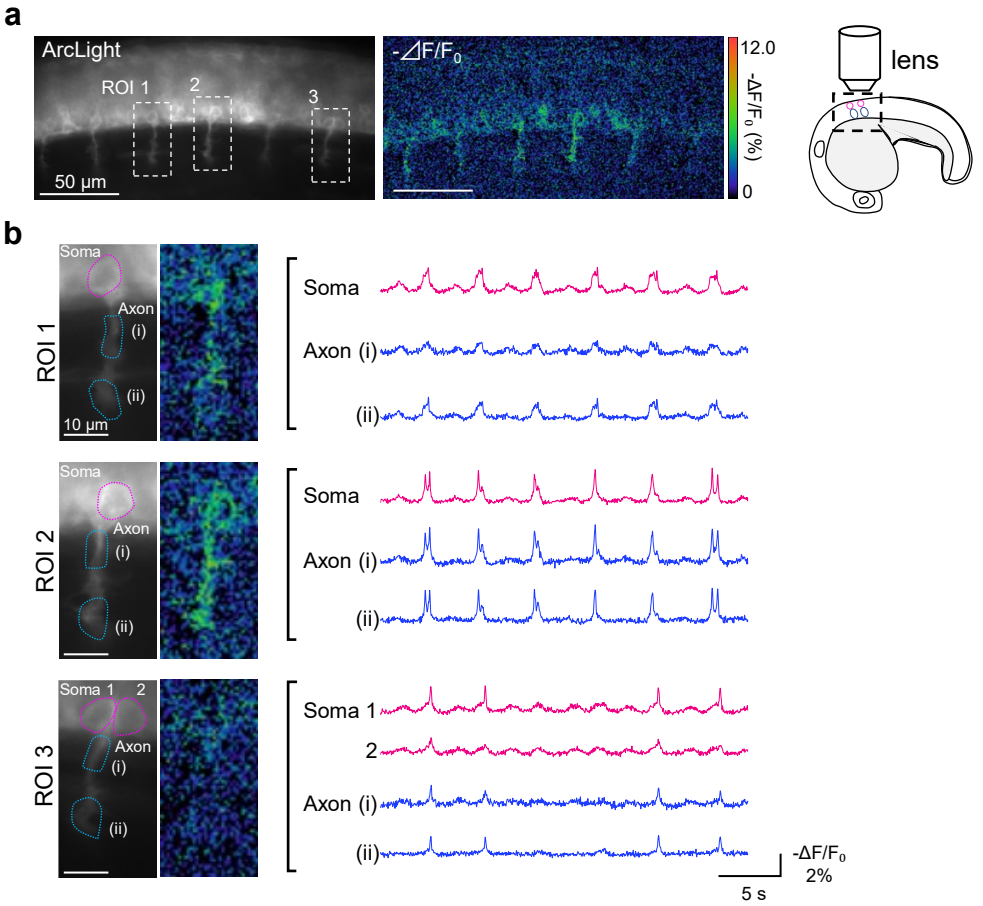
a
ArcLight
ROI 1
2
3
50 μm
-⊿F/F0
12.0
-ΔF/F0 (%)
0
lens
b
ROI 1
Soma
Axon
(i)
(ii)
10 μm
Soma
Axon (i)
(ii)
ROI 2
Soma
Axon
(i)
(ii)
Soma
Axon (i)
(ii)
ROI 3
Soma 1
2
Axon
(i)
(ii)
Soma 1
2
Axon (i)
(ii)
-ΔF/F0
2%
5 s

Figure 4

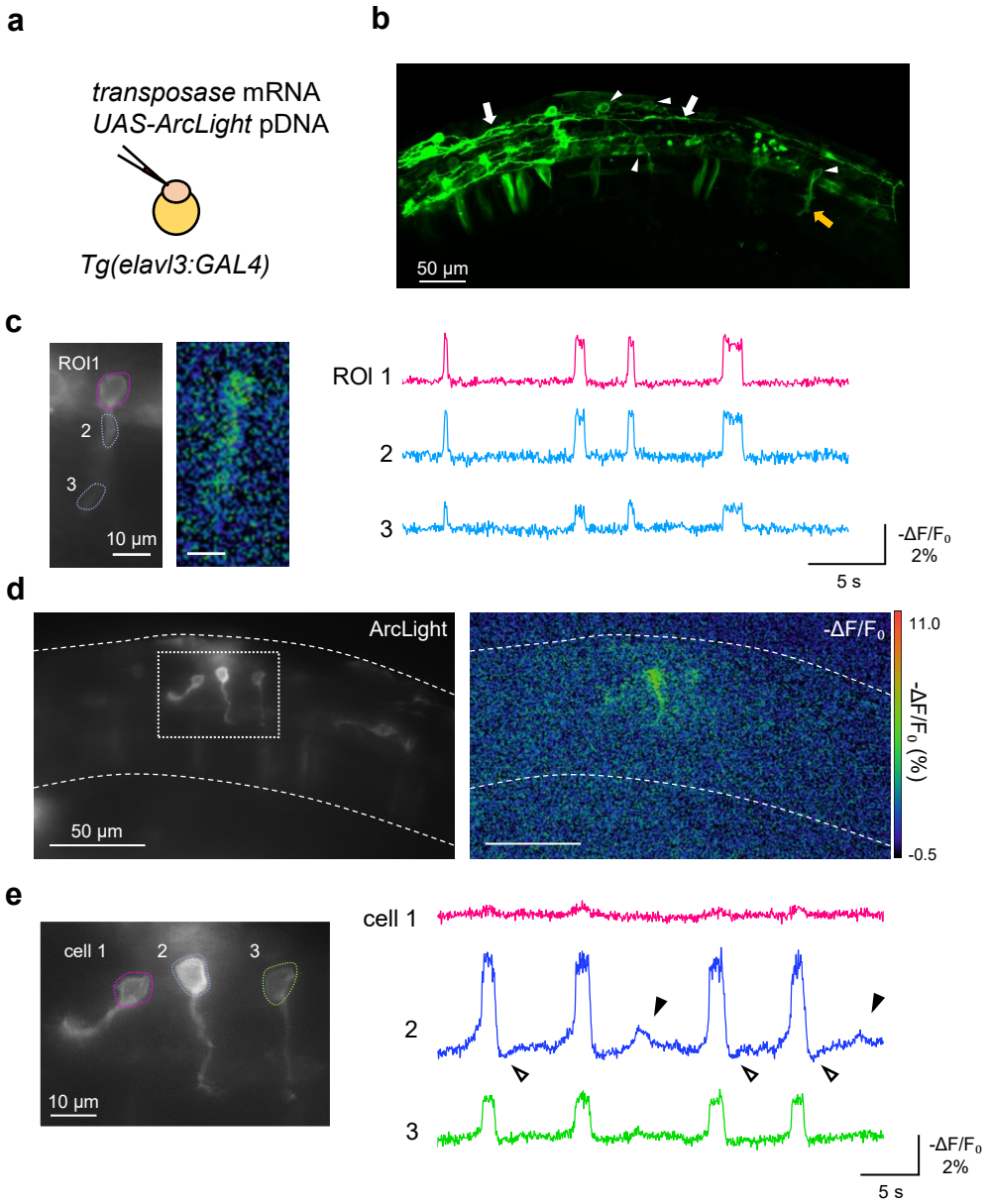
a
transposase mRNA
UAS-ArcLight pDNA
Tg(elavl3:GAL4)
b
50 μm
c
ROI1
2
3
10 μm
ROI 1
2
3
-ΔF/F0
2%
5 s
d
ArcLight
50 μm
-ΔF/F0
11.0
-ΔF/F0 (%)
-0.5
e
cell 1
2
3
10 μm
cell 1
2
3
-ΔF/F0
2%
5 s

Figure 5

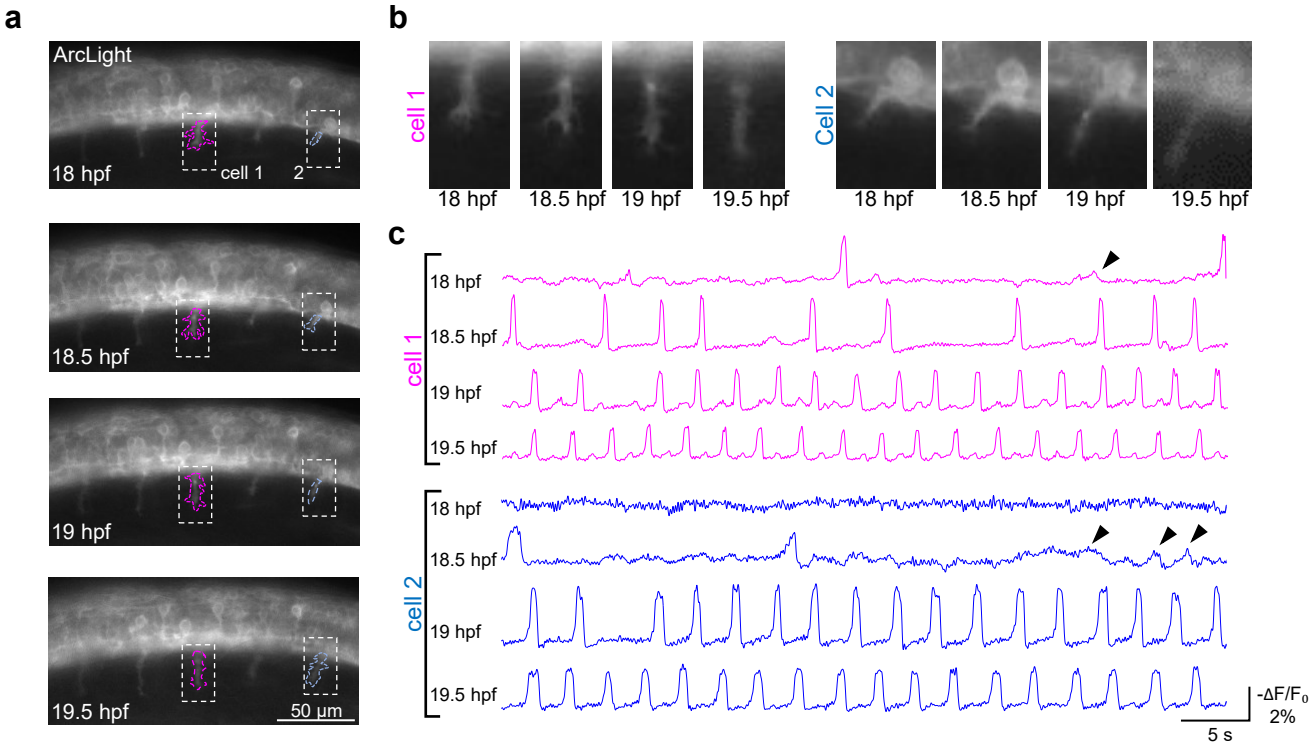
a
ArcLight
18 hpf
cell 1
2
18.5 hpf
19 hpf
19.5 hpf
50 µm
b
cell 1
18 hpf
18.5 hpf
19 hpf
19.5 hpf
Cell 2
18 hpf
18.5 hpf
19 hpf
19.5 hpf
c
cell 1
18 hpf
18.5 hpf
19 hpf
19.5 hpf
cell 2
18 hpf
18.5 hpf
19 hpf
19.5 hpf
-ΔF/F0
2%
5 s

Figure 6

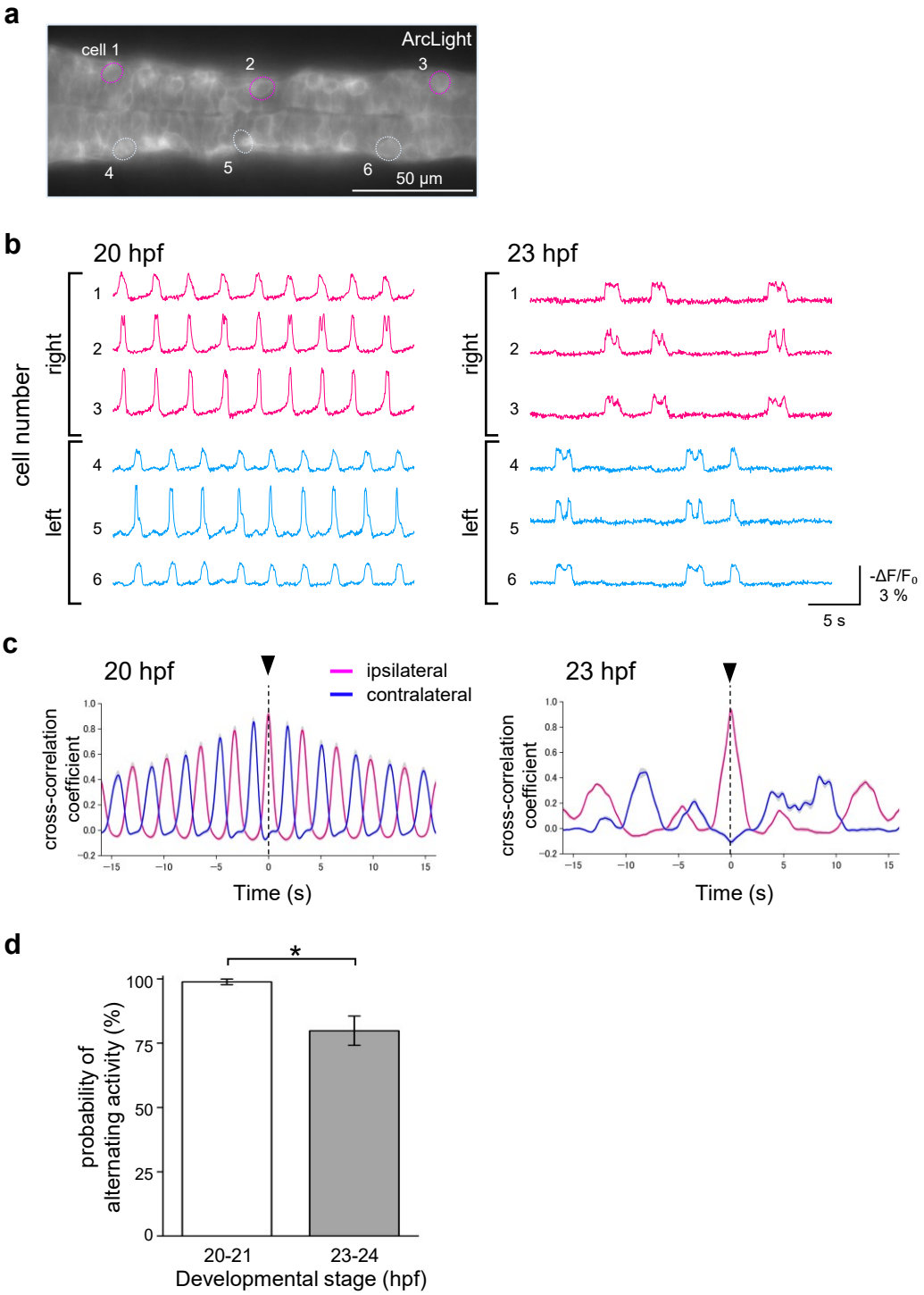
a
cell 1
2
3
4
5
6
ArcLight
50 µm
b
20 hpf
23 hpf
cell number
right
left
1
2
3
4
5
6
-ΔF/F₀
3 %
5 s
c
20 hpf
23 hpf
ipsilateral
contralateral
cross-correlation coefficient
Time (s)
d
probability of alternating activity (%)
100
75
50
25
0
*
20-21
23-24
Developmental stage (hpf)

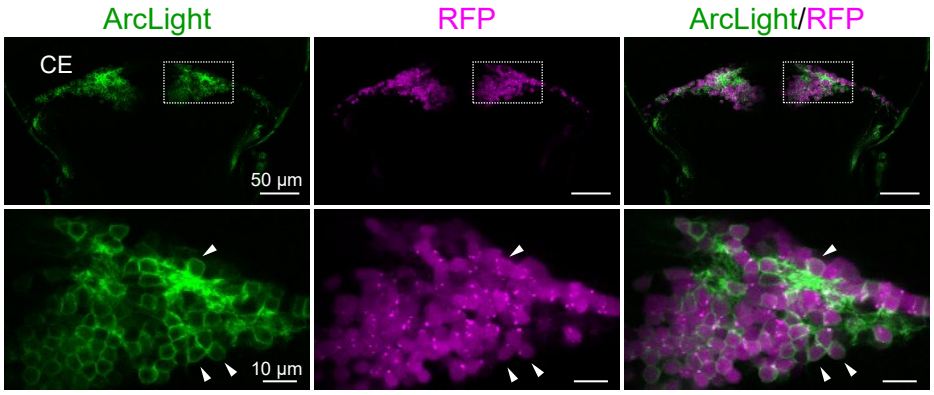

Supplementary Figure S1

a

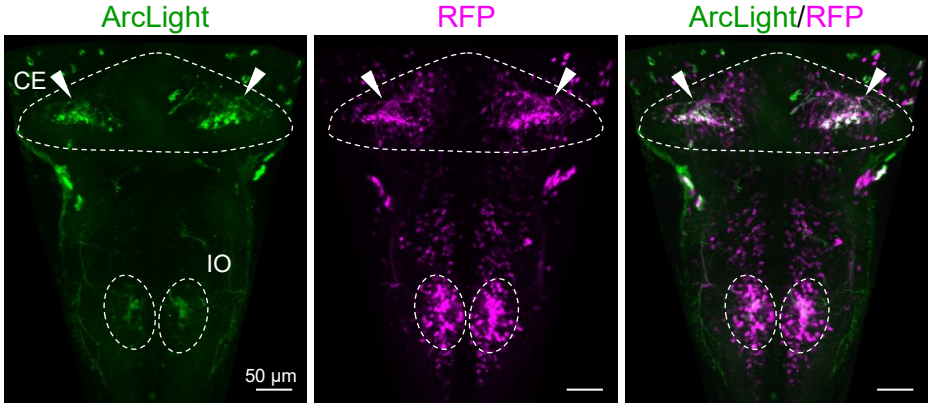

b

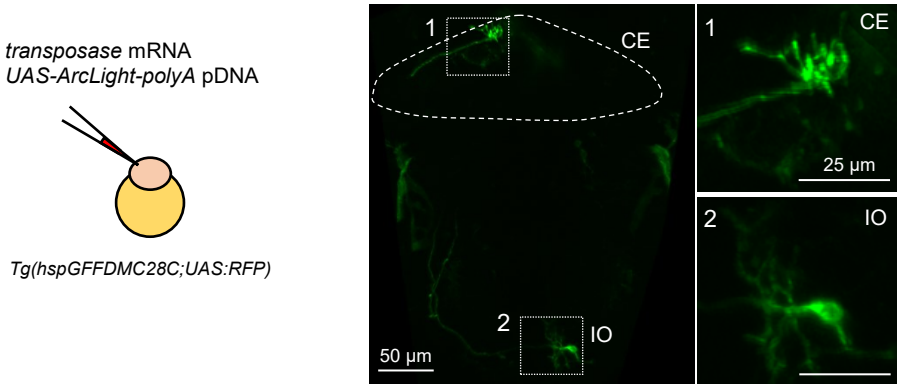

Supplementary Figure S2

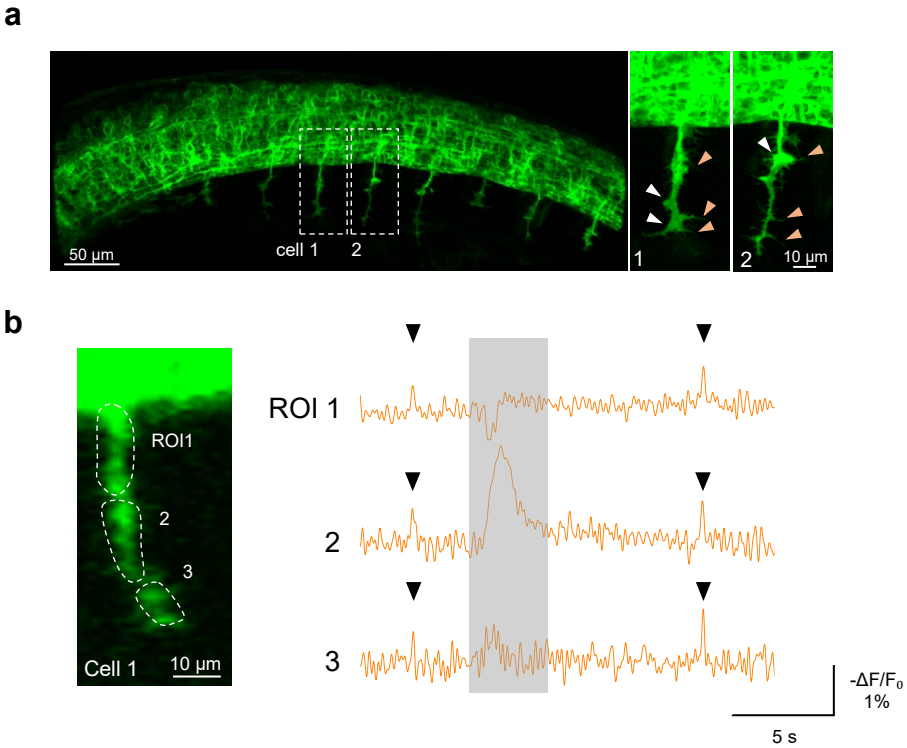

Supplementary Figure S3

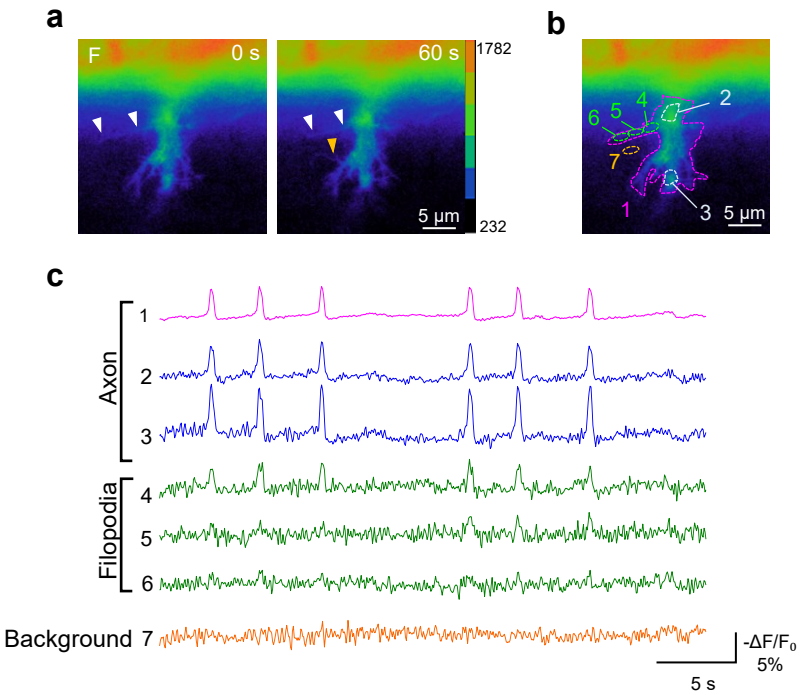

Supplementary Figure S4

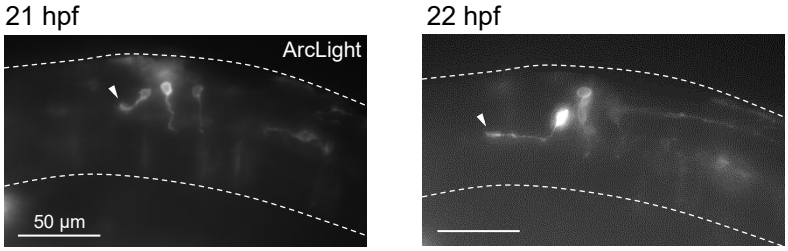

Supplementary Figure S5

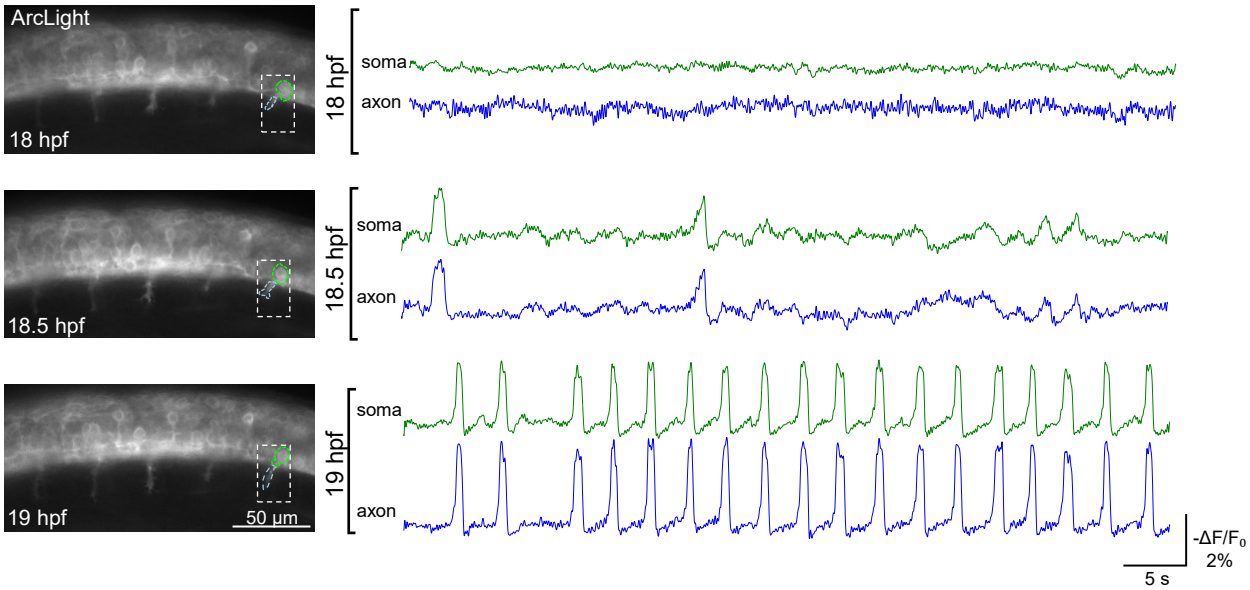

Supplementary Figure S6

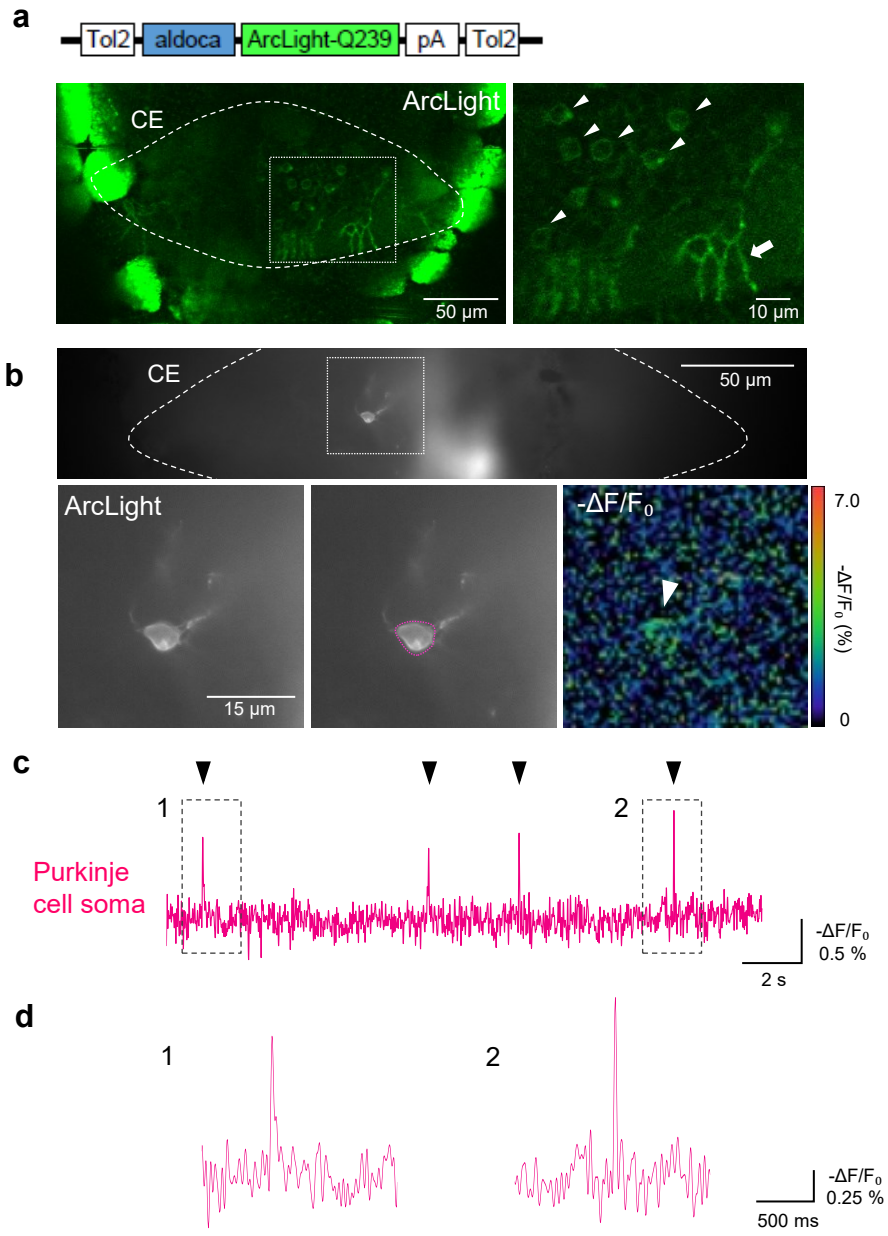

Supplementary Figure S7

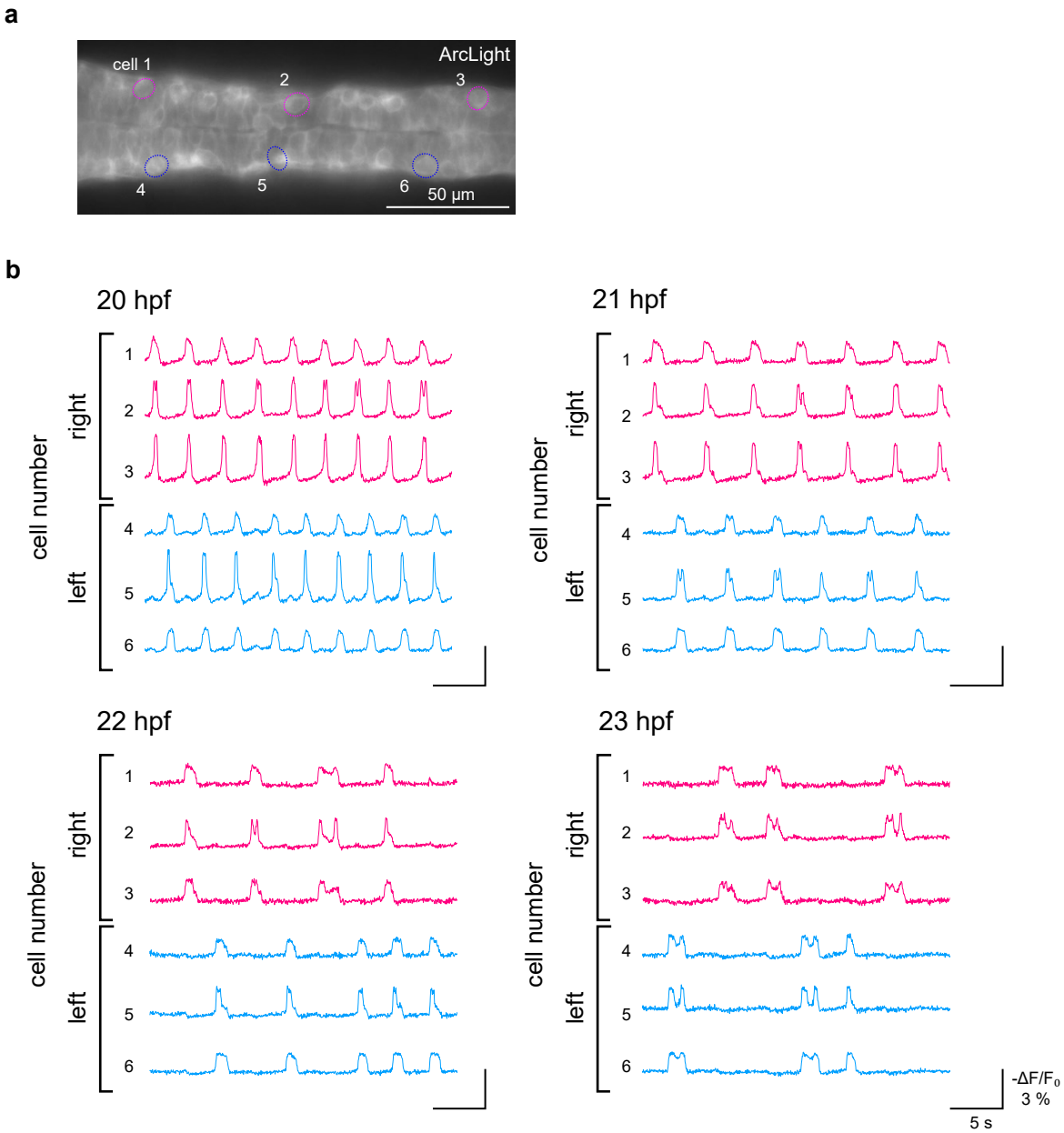

Supplementary Figure S8